# Chapter 11

# Studying Kinetochores In Vivo Using FLIM-FRET

**Tae Yeon Yoo and Daniel J. Needleman**

## Abstract

Kinetochores play essential roles in coordinating mitosis, as a mechanical connector between chromosome and microtubule and as a source of numerous biochemical signals. These mechanical and biochemical behaviors of kinetochores change dynamically in cells during mitosis. Therefore, understanding kinetochore function requires an imaging tool that quantifies the protein–protein interactions or biochemical changes with high spatiotemporal resolution. FRET has previously been used in combination with biosensors to probe protein–protein interactions and biochemical activity. In this chapter, we introduce FLIM-FRET, a lifetime-based method that quantifies FRET, and describe the use of FLIM-FRET as a method for studying dynamic kinetochore behavior in cells with high spatiotemporal resolution.

**Key words** FLIM-FRET, Kinetochore, Bayesian analysis, Live cell imaging

## 1 Introduction

During mitosis, normally functioning eukaryotic cells rapidly and accurately segregate their chromosomes. Inaccurate chromosome segregation gives rise to aneuploidy, which can lead to cancer and death [1, 2]. The proper attachment of microtubules to chromosomes is necessary for accurate chromosome segregation [3, 4]. The interaction between chromosomes and microtubules is predominately mediated by the kinetochore, a highly complex protein structure located at the centromeric region of each chromatid. The main functions of kinetochores can be divided into two parts: attachment and signaling. The kinetochore can attach to microtubules even as the microtubules dynamically switch between growth and shrinking phases. These attachments can withstand significant tension, and therefore provide the physical linkage and coupling between microtubules and chromosomes [5, 6]. The kinetochore is also a source and target of a myriad of regulatory biochemical signals required for the correction of erroneous kinetochore–microtubule attachments and the spindle assembly checkpoint [7–9]. Though both of these main functions of kinetochores are very

Paul Chang and Ryoma Ohi (eds.), *The Mitotic Spindle: Methods and Protocols*, Methods in Molecular Biology, vol. 1413,
DOI 10.1007/978-1-4939-3542-0_11, 

important and have been studied extensively, many aspects of their function and behavior remain poorly understood. One difficulty is a lack of methods for measuring biochemical activities at kinetochore with high temporal and spatial resolution.

Förster Resonance Energy Transfer (FRET) has been widely used as a probe for protein–protein interactions and protein activity in vivo. FRET is the process in which a donor fluorophore transfer the energy from its excited state to an acceptor fluorophore a few nanometers in proximity to the donor. In order to utilize FRET as a probe for protein–protein interaction, one protein of interest is labeled with a donor fluorophore, and the other with an acceptor fluorophore (Fig. 1). FRET can also be used to measure enzyme activity, by adopting FRET biosensors engineered to undergo a conformational change upon the modification by the enzyme of interest, which leads to a change in intramolecular FRET (Fig. 1). Many types of FRET biosensors have been developed and used in a variety of cell biology studies [10–15].

There are two widely used approaches to measure FRET: intensity-based and lifetime-based approaches. Intensity-based approaches include sensitized emission measurements and acceptor photobleaching methods. Though the sensitized emission measurement is the simplest assay to perform, a major limitation is

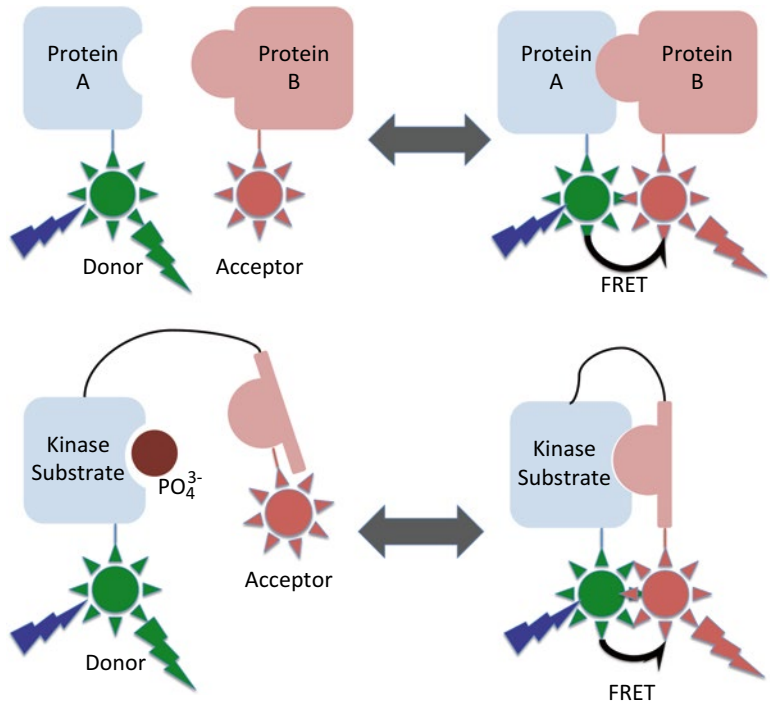


**Fig. 1** The usages of FRET for studying (*top*) protein–protein interaction using fluorophore-labeled proteins, and (*bottom*) kinase activity using engineered FRET bio-sensor

the requirement of complicated correction and normalization procedures and the dependence on the relative concentration of donor and acceptor fluorophores, which is hard to control in practice. The acceptor photobleaching method, on the other hand, does not require the complicated correction procedures, but is difficult to use for time-varying measurements, and is also prone to artifacts due to the motion of acceptors and photodamage from the use of high intensities required for photobleaching. Therefore, this method is not suited for the study of dynamic kinetochores.

Fluorescence Lifetime Imaging (FLIM) is a lifetime-based approach to measure FRET. The fluorescence lifetime refers to the average time that a fluorophore spends in the excited state before relaxing and emitting a photon. The lifetime depends on both its intrinsic photo-physical properties and on its microenvironment, including the local pH, temperature, viscosity, and the presence of quenching, such as by FRET. FLIM-FRET is an imaging and analysis technique that probes fluorophores' lifetimes and quantifies FRET using the measured lifetimes. FLIM-FRET provides a highly quantitative measure of FRET, which is difficult to achieve with intensity-based measurements, because FLIM-FRET uncouples two factors that contribute to the overall FRET signal: the FRET efficiency of an individual FRET pair and the number of FRET pairs. Moreover, FLIM-FRET does not require irreversible reaction, such as acceptor photobleaching, and combined with Bayesian analysis, it is capable of measure FRET with high spatiotemporal resolution. These advantages make FLIM-FRET suitable for the study of dynamic kinetochores in live cell.

Here we describe the Bayesian analysis of FLIM-FRET as a tool to study kinetochore function in live cell at up to sub-millisecond time scales with single kinetochore resolution.

## 2 Materials

### 2.1 Fluorescence Lifetime Imaging (FLIM)

There are several variants of FLIM, which differ in how the fluorescence lifetime is measured and fluorophores are excited. We use time-domain FLIM (vs. frequency-domain) for more straightforward analysis, and two-photon excitation (vs. single-photon excitation) for the flexibility and low photon-induced damage.

(a) Femtosecond Ti:sapphire pulse laser (Mai Tai DeepSee, Spectral Physics)

In time-domain FLIM, an ultrashort pulsed laser is used as an excitation light source. The desired period of the laser is ~10 ns so that the nanosecond-scale fluorescence decay is well captured in a single laser period. Ti:sapphire lasers are particularly convenient when used for two-photon excitation because they are tunable between 690 and 1040 nm, allowing for the use of many different fluorophores.

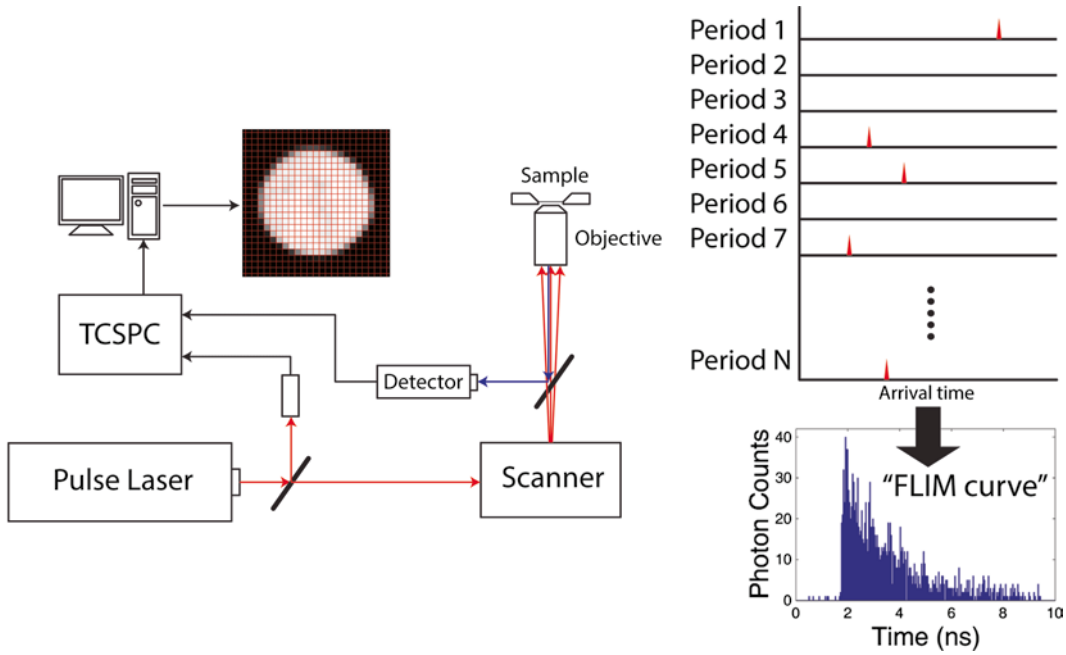


**Fig. 2** (*left*) Arrangement and connections of major components in FLIM system. *Red* and *blue arrows* indicate the path of the excitation laser beam and that of emission photon, respectively. (*right*) Construction of FLIM curve by TCSPC

(b) Time-Correlated Single Photon Counting module (SPC-150, Becker & Hickl GmbH)

Time-Correlated Single Photon Counting (TCSPC) is a technique that detects a single photon and measures the timing of the photon arrival with picosecond time resolution [16]. TCSPC determines the time between the laser pulse and the arrival of the emitted photon at the detector, for each photon detected. After accumulating a number of photons, their arrival times can be used to construct a histogram, called the "fluorescence decay" or "FLIM curve" (Fig. 2)

(c) Laser scanning system (DCS-120, Becker & Hickl GmbH)

(d) Detector (HPM-100-50, Becker & Hickl GmbH)
Time-domain FLIM requires detectors with single-photon sensitivity and fast response.

(e) Optics

All the optics in the excitation light path, including the objective, lenses, and mirrors should be suitable for near-infrared wavelength pulsed laser. For the study of kinetochores, an objective with high Numerical Aperture (NA) is highly preferred because it allows a more compact point spread function (PSF), which results in better spatial resolution as well as more efficient two-photon excitation.

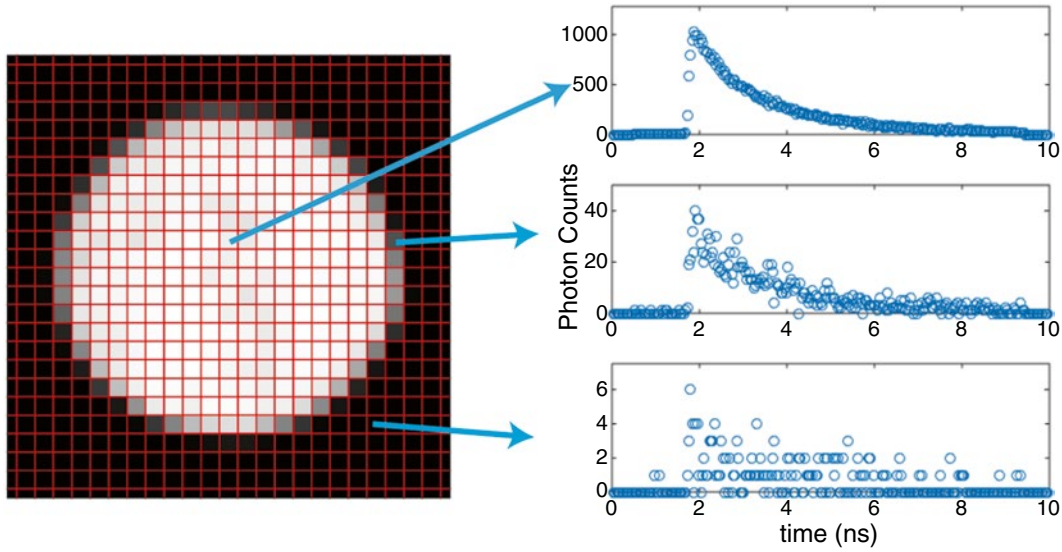


**Fig. 3** Example of FLIM image. (*left*) Intensity image obtained by integrating FLIM curve at each pixel over the arrival time. (*right*) FLIM curves at three different pixels with different number of photons

It is also necessary to have appropriate optics to modulate the excitation intensity. This can be achieved by the combination of polarization optics, neutral density filters, or opto-electronic elements such as a Pockels cell.

(f) FLIM software (SPCM, Becker & Hickl GmbH)
To generate a FLIM image, FLIM software, either custom built or purchased, controls the scanning of the excitation laser over the region of interest and records the pixel location and the arrival time of each emitted photon using TCSPC. A FLIM curve is then generated for each pixel in the image (Fig. 3). These FLIM curves could be analyzed separately or photons from multiple pixels, such as all the pixels from a given kinetochore, could be grouped and analyzed together.

### *2.2 Mitotic Live Cell Imaging*

We use U2OS tissue culture cells, but the protocol can be generalized to any type of cells.

(a) Imaging media (FluoroBrite™ DMEM, Life Technologies)
Imaging media should be carefully selected such that it does not contain significant autofluorescence, while still ensuring cell viability during imaging. The amount of serum should be reduced to a minimal amount, and vitamins such as riboflavin and pyridoxal can be removed completely [17]. Imaging media suited to human tissue culture cells is commercially available. If $CO_2$ control is unavailable, the imaging media should be supplemented with 10 mM HEPES to buffer the cells against changes in the pH.

(b) Sample cover glass (GG-25-pdl, Neuvitro)
Poly-d-lysine coating enhances the attachment and viability of adherent tissue culture cell.

(c) Temperature-controlled microscope sample chamber
We use an open microscope chamber that has electrical temperature control and an aperture where 25 mm round cover glass can be mounted.

(d) Objective heater (Bioptechs)

(e) Objective Z-stage (PIFOC, Physik Instrumente), if 3D imaging is needed.

## 3 Methods

We briefly describe the instrumentation, protocol, and analysis for FLIM-FRET measurement of kinetochores in vivo. More detail on the instrumentation and theory of FLIM-FRET is available in several other publications [16, 18–21].

### 3.1 Two-Photon FLIM Instrumentation

The essential components of a time-domain FLIM system are described in Fig. 2. The optics between the pulse laser and scanning system should be carefully examined and aligned before each experiment, as they influence the spatial resolution and the uniformity of the excitation intensity over the scanning area. The two most important optical components to optimize are the telescope, the combination of lenses that expands or reduces the size of the excitation beam, and the periscope assembly, the combination of mirrors that translates the beam. In order to fully utilize the numerical aperture of the objective, the telescope needs to be adjusted such that the excitation beam is well collimated when entering the objective and large enough to overfill the back aperture of the objective. The periscope assembly should be adjusted such that the beam is perpendicular and centered when entering the objective (*see* **Note 1**).

### 3.2 Live Cell Kinetochore FLIM-FRET Imaging

This section provides step-by-step instruction on live cell kinetochore FLIM-FRET imaging. We present an example using a FRET biosensor for Aurora kinase B activity fused to Hec1, an outer kinetochore protein, in U2OS cells. See Fuller et al. [15] for more information on the Aurora kinase B FRET biosensor.

1. Choice of fluorescent proteins (*see* **Note 2**).
   We chose mTurquiose2 (Cyan) and YPet (Yellow) to be the donor and acceptor fluorescent proteins in the Aurora kinase B FRET reporter. mTurquiose2 is well suited for FLIM-FRET, because of its monoexponential fluorescence decay, long fluorescence lifetime (~4 ns), and excellent brightness with the quantum yield of 93 % [22].

2. Make a plasmid that carries the DNA sequence of the desired kinetochore protein tethered to the FRET probe using standard cloning techniques.
3. Transfect cells.

   Since the brightness of the donor fluorescent protein at kinetochores has influence on the precision of FLIM-FRET measurement, high expression of the labeled protein is preferred as long as overexpression does not affect its behavior. Transient transfection results in some cells having multiple plasmids, which therefore express the construct at very high level. If transient transfection is difficult or undesirable, stable cell lines can be constructed using viruses or genome-editing techniques such as CRISPR.
4. Prepare a sample for imaging by culturing cells on a sample cover glass. Incubate in complete media for about 2 days, at 37 °C, 5 % $CO_2$.
5. Switch the complete growth media to the imaging media 30 min before imaging.
6. Prepare the FLIM setup: turn on and warm up the Ti:sapphire laser, pre-warm the microscope sample chamber and objective lens heater to 37 °C. Check the alignment of the optical system (*see* **Note 1**), and choose a proper emission filter. Calibrate the device that modulates the excitation intensity (*see* **Note 3**).

   The Ti:sapphire laser needs to be set to the optimal two-photon excitation of the donor fluorescent protein, which is 865 nm for mTurquoise2. The optical alignment should always be checked before imaging, since a defective PSF worsens image quality and two-photon excitation efficiency.

   The emission filter must be carefully chosen such to minimize signal from the acceptor, reduce the detected cellular background autofluorescence, and maximize the emission collected from the donor. For the mTurquiose2/YPet pair, we use ET470/40 m filter (Chroma).

   The alignment and other imaging setting should be verified by imaging a standard sample before the experiment (*see* **Note 4**).
7. Mount the sample on the temperature-controlled microscope chamber

   Layer the coverslip with the imaging media that is equilibrated at 37 °C, 5 % $CO_2$, and then cover with mineral oil to prevent evaporation. Clean the bottom of the coverslip with a Kimwipes and ethanol before mounting the chamber to the microscope stage.
8. Acquire FLIM images with the appropriate imaging settings.

   The following is the general guideline of choosing imaging settings: determine the scanning region such that the region of interest just fits into it; using a larger scanning area

will lower the frame rate. The pixel size should be chosen such that each diffraction-limited spot, such as a kinetochore, is composed of about 10 pixels. The integration time should be short enough that moving kinetochores are not blurred, and long enough that more than a few hundreds photons per kinetochore are accumulated and kinetochores are clearly distinguished against the background noise.

For kinetochore imaging of U2OS cells, high quality data can be obtained with an NA 1.25, 40× water-immersion objective, a 14 μm × 14 μm scanning region, 128 × 128 pixels, and a 3–5 s integration time. Smaller regions can be scanned at higher speeds. The repeat time—the time between two consecutive images—will be determined by the aim of the study: studying kinetochore oscillations in metaphase may require a repeat time of 10 s, while for studying long-term changes, a repeat time of a few minutes may be preferable. The excitation beam power is typically set to 1–2 mW. Higher power may induce photodamage, with symptoms including metaphase arrest, prolonged metaphase, shrinkage of the spindle, and an increase in autofluorescence (*see* **Note 5**).

9. Record the instrument response function (IRF) of the FLIM system by measuring second harmonic generation (SHG).

   The IRF plays a very important role in FLIM analysis, and therefore an accurate measurement of the IRF is crucial. The IRF can easily be recorded by measuring second harmonic generation (SHG) signal from a urea crystal. SHG is a nonlinear optical process in which a material that lacks inversion symmetry converts incident photons into photons with half the wavelength of the incident photons. SHG is an ultrafast scattering process so the FLIM curve of SHG provides an accurate measure of the IRF of the FLIM system.

   To make a urea crystal sample for IRF measurements, dissolve urea in water and drop ~10 μl of the urea solution on the coverslip. As the water evaporates, it leaves crystallized urea on the coverslip. Put the coverslip on a microscope slide and seal it. This urea crystal IRF standard can be used repeatedly.

   To record the IRF, set up the emission bandpass filter such that it transmits the photon of the wavelength half of the excitation wavelength. For example, 425/30 can be used for 865 nm excitation. Since the IRF is specific to the imaging settings, every imaging setting other than the emission filter must remain the same. Place the urea crystal on the objective, and park the excitation laser where the crystal generates significant SHG. Make sure that the number of time bins is set to the maximum value. Record SHG for 10–30 s, allowing a smooth IRF curve to be generated. For more information about recording the IRF, refer to the application note published by Becker & Hickl [23] (*see* **Note 6**).

## 3.3 Analysis of Kinetochore FLIM-FRET Imaging

### 3.3.1 FLIM-FRET Models

If there is no donor engaged in FRET, then the number of photons $n(t)$ decays monoexponentially with a long lifetime $\tau_D$:

$$n(t) \propto A \exp\left(-\frac{t}{\tau_D}\right) + (1 - A) \tag{1}$$

where the parameter $A$, which ranges from 0 to 1, determines the fraction of detect photons emitted by the donor. In most applications, the dark noise is low, and thus $A$ is usually very close to 1.

On the other hand, if there is a mixture of donors, with some donors engaged in FRET (all with the same FRET efficiency) and the others not engaging in FRET, then the decay of the number of detected photons is biexponential:

$$n(t) \propto A\left\{f \exp\left(-\frac{t}{\tau_D}\right) + (1 - f)\exp\left(-\frac{t}{\tau_{FRET}}\right)\right\} + (1 - A) \tag{2}$$

where $f$ is the fraction of donors that are not engaged in FRET, and $\tau_D$ and $\tau_{FRET}$ are the lifetimes of donor not in FRET state and in FRET state, respectively. $\tau_D$ and $\tau_{FRET}$ can be translated into the FRET efficiency by:

$$E_{FRET} = 1 - \frac{\tau_{FRET}}{\tau_D} = \frac{1}{1 + \left(\frac{r}{R_0}\right)^6} \tag{3}$$

where $r$ is the separation between donor and acceptor fluorophores and $R_0$ is the Förster radius [24] (*see* **Note 7**).

Figure 4 shows experimentally measured FLIM curves from two samples, where no donors are engaging in FRET and where some donors are in a FRET state. It is apparent that the FLIM curve decays faster when there is FRET, as predicted. Upon closer inspection, it is evident that the data significantly departs from the simple exponential model: the real data appears to be shifted and broadened relative to the model. This discrepancy comes from the limited temporal resolution of the FLIM system and from the finite travel time of photons and information in the system. Fortunately, these discrepancies are determined by the instrument configuration, and can be measured and incorporated into the model. These effects are captured by the instrument response function (IRF), which is what the FLIM system would record from a sample with an infinitely short lifetime. As mentioned above, the IRF can be experimentally measured and usually appears to be a sharp, skewed peak, shifted from $t = 0$ by the same extent as the exponential decay in FLIM curve (Fig. 5).

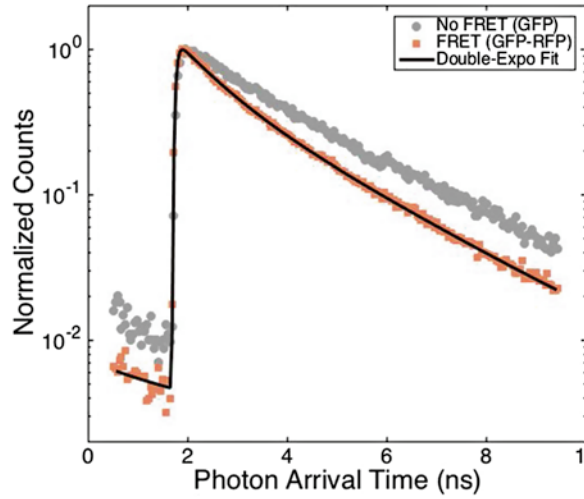


**Fig. 4** Normalized FLIM curve on log-scale of donor when there is no donor engages in FRET (*gray*) and when some fraction of donors are engages in FRET (*orange*)

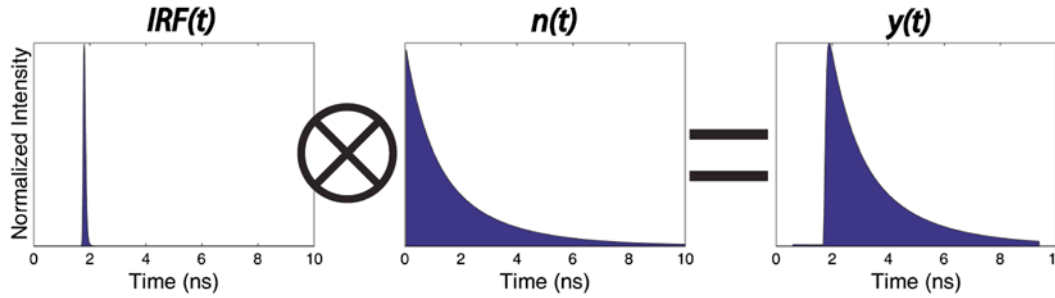


**Fig. 5** The illustration of building a complete FLIM model by convolving IRF and exponential decay model

As illustrated in Fig. 5, a complete FLIM model can be constructed by convolving the exponential decay model (Eqs. 1 or 2) with the measured IRF:

$$y = C_{\text{norm}} \cdot \text{IRF}\left(t - t_s\right) \otimes n\left(t\right) \tag{4}$$

where $C_{\text{norm}}$ is a normalization constant, IRF is the measured instrument response function, $t_s$ is the shift of the measured IRF relative to the real IRF, and $n(t)$ is the exponential decay model given by Eqs. 1 or 2. The shift $t_s$ is necessary for precise fitting because the location of the measured IRF may be different by very small extent, usually within 100 ps, from the real IRF. The constant $C_{\text{norm}}$ is determined by normalizing the area under the curve to the total photon counts. Thus, Eqs. 1 or 2 describes the behav-

ior of the donor fluorophore, while the IRF describes the behavior of the FLIM instrument.

The more realistic model of Eq. 4 is sufficient to describe experimental data. Measured FLIM curves can thus be fit to Eq. 4 to determine the five free parameters: $t_s$, $A$, $\tau_D$, $f$, and $\tau_{FRET}$.

### 3.3.2 Identification and Tracking of Kinetochores

We developed a MATLAB graphical user interface (GUI) that semi-automatically analyzes kinetochore FLIM-FRET data, which allows high-throughput kinetochore analysis.

First, load FLIM images (Fig. 6, *see* **Note 8**). Then identify and track kinetochores using standard particle tracking techniques. We modified the particle tracking MATLAB codes developed and used in Pelletier et al. [25], and incorporated it into the GUI. As shown in Fig. 6b, each kinetochore trajectory is automatically labeled with a number, and the GUI enables us to manually modify mislabelled kinetochore features, or remove features that are incorrectly identified as kinetochores. By fitting 2D Gaussian to each kinetochore, the location of the kinetochore can be determined with sub-pixel precision, and can be used for distance and velocity measurements.

### 3.3.3 FLIM-FRET Measurement of Kinetochore with Bayesian Analysis

Assuming that the fluorescence lifetimes of FRET and non-FRET states are constant throughout the movie, we can precisely determine the lifetimes by grouping all the FLIM curves from the kinetochores in every image to obtain a FLIM curve with a large number of photons (Fig. 6c), and make inference using the biexponential FLIM model to accurately estimate the fluorescence lifetimes (Fig. 6d). In the analysis of FLIM curves in each frame or each kinetochore with a fewer number of photons, we can then fix the lifetimes and IRF shift to the values obtained from the sum of many FLIM curves, and perform the biexponential FLIM-FRET Bayesian analysis with a reduced number of free parameters to precisely measure the fraction of the donors FRETing at each timepoint or at each kinetochore (Fig. 6e, f).

Getting accurate and precise estimation of parameters in a biexponential FLIM-FRET model is not a simple task, especially when the number of photons composing the FLIM curve is small. When the number of photons is of the order of $10^5$ or more, commonly used nonlinear least-square fitting of the Eq. 4 may provide the estimates of the FLIM parameters with reasonable accuracy and small bias. However, when the number of photons is very limted, which is the case for the study of dynamic kinetochores, a Bayesian approach with a complete probabilistic model must be employeed, in order to minimize the bias resulting from the simplified assumption inherent to least-square fitting.

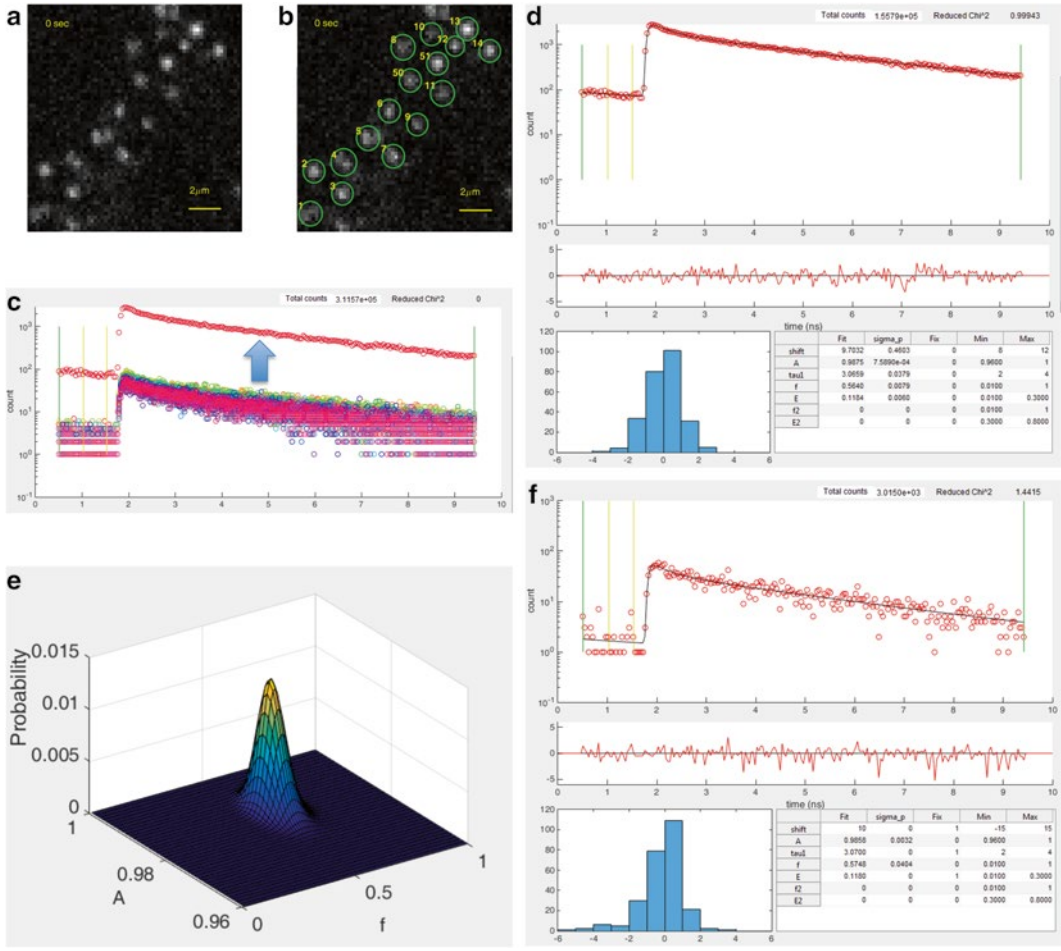


**Fig. 6** Kinetochore FLIM-FRET measurement procedures. (a) Loading FLIM images saved in a special data format. (b) Identification of kinetochores. (c) Summing the FLIM curves obtained from every kinetochore, and (d) determination of the fluorescence lifetimes. (e, f) Bayesian FLIM analysis on the FLIM curve from one frame

Let $\theta$ be the set of parameters that governs the FLIM model, and $y = \{yi\}$ be the observed FLIM data, where $yi$ is the number of photons detected in $i$-th time bin of the FLIM curve. The aim of Bayesian inference is to obtain the posterior probability distribution of the parameters of interest, $p(\theta \mid y)$, through the Bayes rule:

$$p(\theta \mid y) \propto p(y \mid \theta)\, p(\theta) \tag{5}$$

The common name of the first term in the product $p(y \mid \theta)$ is the "likelihood function," which is the probability of the observed data $y$ given the parameter values $\theta$. The likelihood function is based on the data generation process. Let $\Delta t$ be the width of the time bin with which the FLIM data is acquired. Then the likelihood function can be written as

$$p(y\,|\,\theta) \propto \prod_{i=1}^{N} P\left(t_{\mathrm{ar}} \in \left[(i-1)\Delta t, i\Delta t\right]\,|\,\theta\right)^{y_i} \tag{6}$$

where $t_{\mathrm{ar}}$ is the photon arrival time, and $N$ is the number of time bins. Assuming that the size of the time bin is very small compared to the time scale of fluorescence decay, the probability that the arrival time $t_{\mathrm{ar}}$ falls in the $i$-th time bin is approximated by a Riemann sum:

$$P\left(t_{\mathrm{ar}} \in \left[(i-1)\Delta t, i\Delta t\right]\,|\,\theta\right) \cong \sum_{k=(i-1)K+1}^{k=iK} h_\theta\left(k\,\Delta t\right)\Delta t \tag{7}$$

where $\tilde{\Delta} t$ is the smallest time bins with which IRF is measured, and the ratio $K = \dfrac{\Delta t}{\Delta \tilde{t}}$ is a positive integer. $h_\theta\left(k\Delta\tilde{t}\right)$ in the Eq. 7 can be written as:

$$h_\theta\left(k\,\tilde{\Delta} t\right) = \left(\mathrm{IRF} \otimes \left(Ag_\theta + (1-A)\right)\right)\left(k\,\tilde{\Delta} t\right) \cong \sum_{l} \mathrm{mIRF}\left[l - b_{\mathrm{shift}}\right]\left(Ag_\theta\left((k-l)\,\tilde{\Delta} t\right) + (1-A)\right) \tag{8}$$

where mIRF is the IRF measured in the finest time bins with size $\Delta\tilde{t}$ , and $b_{\mathrm{shift}}$ is an integer parameter that determines the approximate shift of measured IRF from the theoretical IRF. The function $g\theta$ depends on the number of exponentials in FLIM model. For example, when there are two species of donors, one of which are engaged in FRET with the same efficiency and the other not, $g\theta$ is expressed as:

$$g_\theta\left(t_{\mathrm{d}}\right) = f\,\mathrm{e}^{-\frac{t_{\mathrm{d}}}{\tau_{\mathrm{D}}}} + (1-f)\,\mathrm{e}^{-\frac{t_{\mathrm{d}}}{\tau_{\mathrm{FRET}}}} \tag{9}$$

We ignored the "pile-up" effect that results from photons that are emitted from the fluorophores excited in the previous pulses and appear in the current laser period, as typically this effect is very small for commonly used fluorophores with lifetime shorter than 4 ns [16]. Equation 8 can be efficiently evaluated by using a fast convolution algorithm combined with fast Fourier transformation, rather than directly carrying out the summation.

The Bayes rule (Eq. 5) results in the posterior distribution:

$$p(\theta\,|\,y) \propto p(\theta) \prod_{i=1}^{N} P\left(t_{\mathrm{ar}} \in \left[(i-1)\Delta t, i\Delta t\right]\,|\,\theta\right)^{y_i} \tag{10}$$

The prior distribution $p(\theta)$ is often chosen to be flat between reasonable upper and lower limits of the parameters, i.e., $p(\theta) = 1$ (*see* **Note 9**).

Equation 10 needs to be numerically evaluated, which can be done using a number of different methods. The grid search method is conceptually simple to implement. In this method, a grid is

formed by dividing the range of values for each of parameter in $\theta = \{b_{\text{shift}}, A, f, \tau_D, \tau_{FRET}\}$ into a number of discrete levels, and the posterior distribution is computed at each grid point. The computation time grows exponentially with the number of free parameters, and therefore the use of this method is restricted to low-dimensional searches. For example, if the values of $b_{\text{shift}}$, $\tau_D$, and $\tau_{FRET}$ are known, and a search is performed over the other two parameters, this method works well with a reasonably fine grid and a computation time of few seconds. On the other hand, if there are many free parameters, Markov Chain Monte Carlo (MCMC) is a faster method. The most popular variants of MCMC are Gibbs sampling and Metropolis–Hastings algorithm [26–29]. We do not discuss the details of these algorithms here. Figure 7 shows the marginal posterior distributions constructed by the grid search and Gibbs sampling, when only $b_{\text{shift}}$ is fixed and the other four parameters are free. The two methods produced almost identical result, while the Gibbs sampling is roughly ten times faster than the grid search, taking ~10 min vs. ~100 min to run.

Once the posterior distribution is calculated, a variety of point and interval estimations of the parameters can readily be made. If the marginalized posterior distribution of a parameter is symmetric, its mean is a natural point estimate for the parameter. If the marginalized posterior distribution is truncated or asymmetric, the posterior mode may be a better point estimate. The Bayesian probability interval, or credible interval, can be also found from the marginal posterior distribution and be used as an interval estimate of parameter.

One essential advantage of using Bayesian analysis is its explicit use of probability for quantifying uncertainty in inferences. This makes the propagation of uncertainty perspicuous, especially when combining estimates from multiple datasets. Another important advantage of Bayesian FLIM analysis is its superior accuracy and precision compared to other fitting methods. It has been shown that Bayesian analysis can be used to determine fluorescence lifetimes of a monoexponential fluorescence decay with no bias with as little as 50 photons, while LS and MLE cause significant bias at such low photon counts [30]. We also confirmed that when applied to double-exponential fluorescence decay data Bayesian FLIM analysis is capable of estimating the fraction of one exponential component relative to the other with no bias with only 200 photons. Using standard labeling levels and illumination intensities, one photon can be collected from a single kinetochore every microsecond. Thus, with Bayesian FLIM analysis it should be possible to measure the fraction of fluorophores engaged in FRET at a single kinetochore every 200 μs, enabling the study of submillisecond dynamics of protein behaviors at kinetochores.

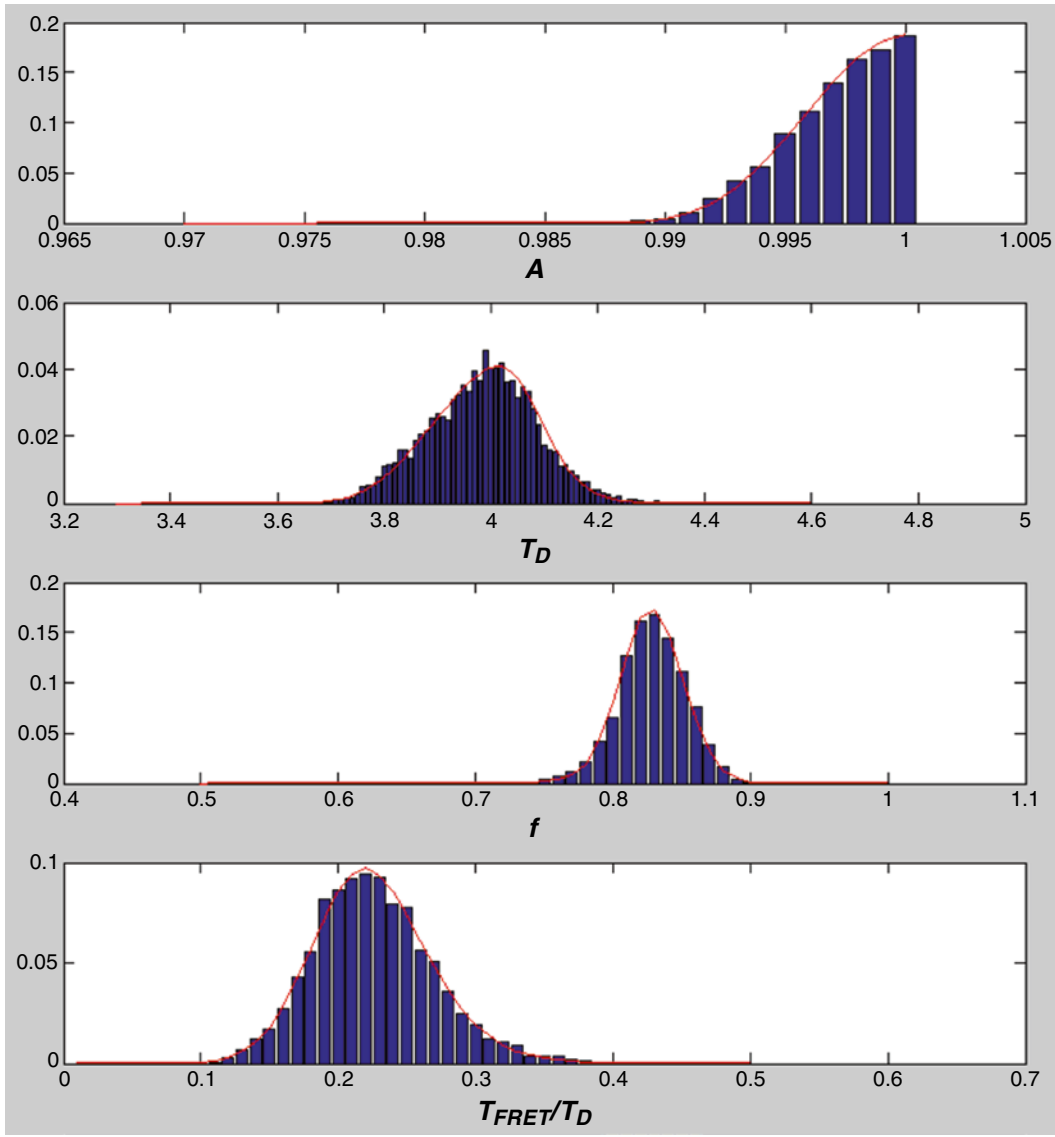


**Fig. 7** Marginal posterior distribution constructed by the grid search (*red line*) and Gibbs sampling (*blue bar*). The sizes of the grid are 0.001 for *A*, and 0.01 for the other three parameters. 5000 values were stimulated by Gibbs sampling

## 4 Notes

1. Some alignment tools can facilitate the adjustment and alignment of the periscope and telescope assembly. Fluorescing alignment disks (such as VRC2RMS, Thorlabs), which can be mounted on the nose piece of microscope, is particularly useful as it can be used to visualize the size and position of the beam entering the objective. We also use a fluorescing alignment disk in combination with a long lens tube (such as SM1E60, Thorlabs) to ensure the perpendicularity and collimation of

the excitation beam. To achieve perpendicularity, we adjust the periscope assembly such that the beam is centered on the alignment disk when the disk is mounted on the nose piece and when it is mounted on a lens tube that is installed on the nose piece (i.e., the alignment disk is positioned away from the nose piece by the length of the lens tube). To achieve collimation, we adjust the telescope assembly such that the size of the beam is the same at the nose piece and away from the nose piece.

2. The most important factor to consider when choosing a donor fluorescent protein is the complexity of the donor's fluorescence decay. Some fluorescent proteins, such as ECFP and EYFP, exhibit multiexponential fluorescence decay even in the non-FRETing state. Multiexponential fluorescence decay greatly complicates the analysis and interpretation of FLIM data. Therefore, it is essential to verify a mono-exponential fluorescence decay of the donor fluorescent protein through negative controls. A proper negative control is the donor fluorescent protein targeted to the same protein as the FRET probe, so that the local environmental effects on the fluorescence decay can be investigated in advance of the FRET measurements. As in other fluorescence microscopies, brightness and photostability are also important, since the number of photons determines the precision of FLIM-FRET measurement.

   The acceptor fluorescent protein should be chosen such that the Förster radius is large enough that the FRETing and non-FRETing states can be easily distinguished. Another important factor to consider is the maturation time of the acceptor fluorescent protein. Slow maturation leads to a large fraction of acceptors being unfolded or immature, and therefore results in the reduction of the number of donor molecules that can engage in FRET. The photostability of the acceptor is also essential for prolonged imaging, but the brightness of the acceptor is not crucial, since emission from the acceptor is not measured in FLIM-FRET.

3. We place a linear polarizer, a motorized half-wavelength plate and another linear polarizer in series in the laser path to modulate the excitation intensity; the transmission of the laser changes as the angle of the half-wavelength plate changes. Before every experiment, we create a mapping between the angle of the half-wavelength plate and the excitation laser intensity, by measuring the laser power at the objective lens.

4. We normally use Alexa dye on a coverslip to check the uniformity of the excitation, and 200 nm fluorescent microsphere (T14792, Life Technologies) to check the quality of the point spread function. When the system is aligned properly, the full width at half maximum of the point spread function should be ~300 nm laterally and ~700 nm axially.

5. In order to prevent the emergence of artifacts related to photodamage and photobleaching, one should carefully choose

appropriate imaging settings by performing negative control experiments. The best negative control sample is cells expressing the protein of interest labeled with only the donor. To test an imaging setting, take images of the negative control sample with the imaging setting, and check whether the observed fluorescence lifetime and/or brightness of the donors change over time. Photodamage is known to result in the increase in autofluorescence [31], which contaminates the fluorescence signal from donor and may change the observed fluorescence lifetime. Photobleaching also may change the observed fluorescence lifetime as it increases the relative contribution of the autofluorescence. Photodamage and photobleaching are highly nonlinear with excitation intensity, following a power law with the exponent greater than 2, while the two-photon excitation is proportional to intensity squared [32, 33]. Therefore, photodamage and bleaching can be significantly suppressed by lowering the excitation intensity, without sacrificing the fluorescence signal from the donor as much. For this reason, as a way to enhance the signal-to-noise ratio, using longer integration time is preferred over using higher excitation intensity.

6. When acquiring the IRF using an SHG sample, remove the condenser lens because it may reflect the SHG and cause additional peak in the measured IRF curve.
7. It is not recommended to use Eq. 3 to attempt to measure the distance between donor and acceptor fluorophores. One major difficulty is that FRET efficiency is highly dependent on the relative orientation of the donor and acceptor fluorophores. The distance-FRET efficiency predicted by Eq. 3 holds only for FRET efficiency averaged over all orientations, assuming that the orientations are isotropic. In practice, it is difficult to know the relative orientations of the donor and acceptor.
8. The MATLAB code that imports FLIM data generated by Becker & Hickl SPCM software is available from Becker & Hickl upon request.
9. Any prior knowledge can be incorporated into the posterior distribution through the prior distribution. For example, some studies impose an exponential prior on the lifetime [30], i.e., $p(\theta)=\alpha e^{-\alpha\tau}$.

## References


1. Gordon DJ, Resio B, Pellman D (2012) Causes and consequences of aneuploidy in cancer. Nat Rev Genet 13:189. doi:10.1038/nrg3123
2. Rajagopalan H, Lengauer C (2004) Aneuploidy and cancer. Nature 432:338–341
3. Bakhoum SF, Thompson SL, Manning AL (2009) Genome stability is ensured by temporal control of kinetochore–microtubule dynamics. Nat Cell Biol 11:27. doi:10.1038/ncb1809
4. Cimini D, Degrassi F (2005) Aneuploidy: a matter of bad connections. Trends Cell Biol 15:442, http://www.sciencedirect.com/science/article/pii/S0962892405001601
5. Nicklas RB (1983) Measurements of the force produced by the mitotic spindle in anaphase. J Cell Biol 97:542. doi:10.1083/jcb.97.2.542
6. Inoué S, Salmon ED (1995) Force generation by microtubule assembly/disassembly in mito-

sis and related movements. Mol Biol Cell 6:1619. doi:10.1091/mbc.6.12.1619
7. Li R, Murray AW (1991) Feedback control of mitosis in budding yeast. Cell 66:519–531
8. Musacchio A, Salmon E (2007) The spindle-assembly checkpoint in space and time. Nat Rev Mol Cell Biol 8:379–393
9. Godek KM, Kabeche L, Compton DA (2015) Regulation of kinetochore-microtubule atta chments through homeostatic control during mitosis. Nat Rev Mol Cell Biol 16:57. doi:10.1038/nrm3916
10. Violin JD, Zhang J, Tsien RY, Newton AC (2003) A genetically encoded fluorescent reporter reveals oscillatory phosphorylation by protein kinase C. J Cell Biol 161:899–909
11. Chen Y, Saulnier J, Yellen G, Sabatini B (2014) A PKA activity sensor for quantitative analysis of endogenous GPCR signaling via 2-photon FRET-FLIM imaging. Front Pharmacol 5:56
12. Espenel C, Acharya BR, Kreitzer G (2013) A biosensor of local kinesin activity reveals roles of PKC and EB1 in KIF17 activation. J Cell Biol 203:445–455
13. Pereira AM, Tudor C, Kanger JS, Subramaniam V, Martin-Blanco E (2011) Integrin-dependent activation of the JNK signaling pathway by mechanical stress. PLoS One 6:e26182
14. Gavet O, Pines J (2010) Progressive activation of CyclinB1-Cdk1 coordinates entry to mitosis. Dev Cell 18:533–543
15. Fuller B et al (2008) Midzone activation of aurora B in anaphase produces an intracellular phosphorylation gradient. Nature 453:1132–1136
16. Becker W (2012) The bh TCSPC handbook. Becker & Hickl GmbH, Berlin
17. Bogdanov A, Kudryavtseva E, Lukyanov K (2012) Anti-fading media for live cell GFP imaging. PLoS One 7:e53004
18. Lleres D, Swift S, Lamond AI (2007) Detecting protein-protein interactions in vivo with FRET using multiphoton fluorescence lifetime imaging microscopy (FLIM). Curr Protoc Cytom. doi: 10.1002/0471142956.cy1210s42
19. Berezin M, Achilefu S (2010) Fluorescence lifetime measurements and biological imaging. Chem Rev 110:2641–2684
20. Festy F, Ameer-Beg S, Ng T, Suhling K (2007) Imaging proteins in vivo using fluorescence lifetime microscopy. Mol Biosyst 3:381–391
21. Ebrecht R, Paul C, Wouters F (2014) Fluorescence lifetime imaging microscopy in the medical sciences. Protoplasma 251:293305
22. Goedhart J et al (2011) Structure-guided evolution of cyan fluorescent proteins towards a quantum yield of 93%. Nat Commun 3:751
23. Becker & Hickl GmbH (2008) Recording the Instrument Response Function of a Multiphoton FLIM System
24. Lakowicz JR (2011) Principles of fluorescence spectroscopy, vol 954. Springer, New York, NY
25. Pelletier V, Gal N, Fournier P, Kilfoil M (2009) Microrheology of microtubule solutions and actin-microtubule composite networks. Phys Rev Lett 102:188303
26. Casella G, George EI (1992) Explaining the Gibbs sampler. Am Stat 46:167. doi:10.1080/00031305.1992.10475878
27. Geman S, Geman D (1984) Stochastic relaxation, gibbs distributions, and the Bayesian restoration of images. IEEE Trans Pattern Anal Mach Intell PAMI-6:721–741
28. Gelman A et al (2013) Bayesian data analysis, vol 675. Chapman and Hall/CRC, Boca Raton, FL
29. Lawrence CE et al (1993) Detecting subtle sequence signals: a gibbs sampling strategy for multiple alignment. Science 262:208–214
30. Rowley M, Barber P, Coolen ACC, Vojnovic B (2011) Bayesian analysis of fluorescence lifetime imaging data. Proc SPIE 7903:790325-1
31. Galli R et al (2014) Intrinsic indicator of photodamage during label-free multiphoton microscopy of cells and tissues. PLoS One 9:e110295
32. Hopt A, Neher E (2001) Highly nonlinear photodamage in two-photon fluorescence microscopy. Biophys J 80:2029
33. Patterson G, Piston D (2000) Photobleaching in two-photon excitation microscopy. Biophys J 78(4):2159